PHYSICAL REVIEW MATERIALS **4**, 074401 (2020)

Structural, magnetic, transport, and thermoelectric properties of the pseudobrookite $AlTi_2O_5$-Ti_3O_5 system

Ryusei Takahama,[1] Toi Ishii,[1] Daigo Indo,[1] Mitsutoshi Arizono,[1] Chieko Terakura,[2] Yoshinori Tokura,[2,3] Nao Takeshita,[4]
Masaaki Noda,[5] Hideki Kuwahara,[5] Takuo Saiki,[6] Takuro Katsufuji,[6] Ryoichi Kajimoto,[7] and Tetsuji Okuda[1,*]
[1]*Graduate School of Science and Engineering, Kagoshima University, Kagoshima 890-0065, Japan*
[2]*RIKEN Center for Emergent Matter Science, Wako 351-0198, Japan*
[3]*Department of Applied Physics and Tokyo College, University of Tokyo, Tokyo 113-8656, Japan*
[4]*National Institute of Advanced Industrial Science and Technology, Tsukuba 305-8568, Japan*
[5]*Department of Physics, Sophia University, Chiyoda-ku, Tokyo 102-8554, Japan*
[6]*Department of Physics, Waseda University, Tokyo 169-8555, Japan*
[7]*Materials and Life Science Division, J-PARC Center, Tokai, Ibaraki 319-1195, Japan*

(Received 12 November 2019; revised 25 May 2020; accepted 5 June 2020; published 6 July 2020)

We investigated the structural, magnetic, transport, and high-temperature thermoelectric properties of single crystals of the pseudobrookite $Al_{1-x}Ti_{2+x}O_5$ for $0 \leqslant x \leqslant 1$ grown using a floating zone. We found a correlation of spin-singlet Ti^{3+}-Ti^{3+} dimers coupled with the lattice even in the conductive α and λ phases which develops with increasing x. This developing dimer correlation reduces the number of unpaired Ti^{3+} ions, which makes the compound more conductive owing to the suppression of disorder for x up to about 0.75. The dimer fluctuation causes a critical enhancement of the magnetic susceptibility at around 150 K in the λ phase near the boundary ($x \sim 0.9$) between the λ and the β phases. Such a correlation of the spin-singlet Ti^{3+}-Ti^{3+} dimers may produce a high Seebeck coefficient in the conductive α and λ phases leading to a large thermoelectric power factor at high temperatures.

DOI: 10.1103/PhysRevMaterials.4.074401

I. INTRODUCTION

The pseudobrookite Ti_3O_5 has the same chemical formula (Ti_nO_{2n-1} for $n = 3$) as that of the Magnéli phase (Ti_nO_{2n-1} for $n \geqslant 4$) and has various polymorphisms called α, β, γ, δ, and λ phases [1–7]. The polymorphisms of Ti_3O_5 are classified into two groups: the α, β, and λ phases in one group, and the γ and δ phases in the other. In bulk samples of the former group, the structural phase transition [1,2,4] from the low-temperature (low-T) monoclinic β phase (space-group $C2/m$) to the intermediate monoclinic λ phase (space-group $C2/m$) occurs at about 460 K on heating, and the transition from the λ phase to the high-temperature (high-T) orthorhombic α phase (space-group $Cmcm$) occurs at about 500 K. In bulk samples of the latter group, the structural phase transition [3,6] from the monoclinic γ phase (space-group $I2/c$) to the monoclinic δ phase (space-group $P2/a$) occurs at about 240 K on cooling.

It is reported that a charge ordering of Ti^{3+} ($3d^1$, spin 1/2) and Ti^{4+} ($3d^0$, spin 0) occurs in β-Ti_3O_5 [1,2,4] and in Magnéli Ti_4O_7 [7–10], where Ti^{3+} ions are dimerized to form nonmagnetic spin-singlet dimers accompanying the local lattice deformation. As the temperature T increases, a first-order transition from the nonmagnetic spin-singlet state to the paramagnetic charge-delocalized mixed-valent state occurs [4,5] simultaneously with a first-order structural phase transition from the β phase to the λ phase accompanying abrupt changes in the lattice parameters. The magnetic state does not significantly change [4,5] during the second-order structural phase transition [5] from the λ to the α phases. The electric resistivity dramatically changes to the more conductive state at the first-order transition from the β to the λ phases. The resistivity does not show an abrupt change at the transition from the λ to the α phase, although the resistivities in all phases show some semiconducting behaviors. It is also reported that Ti_3O_5 nanocrystals [5] are in the intermediate paramagnetic λ phase at room temperature (RT) and show a reversible photoinduced phase transition between the λ and β phases at RT.

This successive transition of Ti_3O_5 is similar to that of Ti_4O_7, whose low-T phase is also in a charge-ordered state with Ti^{3+}-Ti^{3+} dimers and undimerized Ti^{4+} [8,9]. However, the intermediate semiconducting state of Ti_4O_7 is still in a nonmagnetic state, which implies a dynamically disordered spin-singlet dimer state called a bipolaron spin liquid state [9]. Soft and hard x-ray photoemission spectroscopy measurements suggest an anomalous state with a pseudogap coexisting with a remnant coherent state [10].

However, polycrystalline α-$AlTi_2O_5$ has recently been synthesized, and its electronic structure has been calculated via first principles [11]. The formal valence of the Ti ion in this compound is +3.5, which is the same as that of Ti_4O_7. A charge-density-wave (CDW) state has been proposed on the basis of spin and charge susceptibilities calculated using the

---

[*] okuda@eee.kagoshima-u.ac.jp

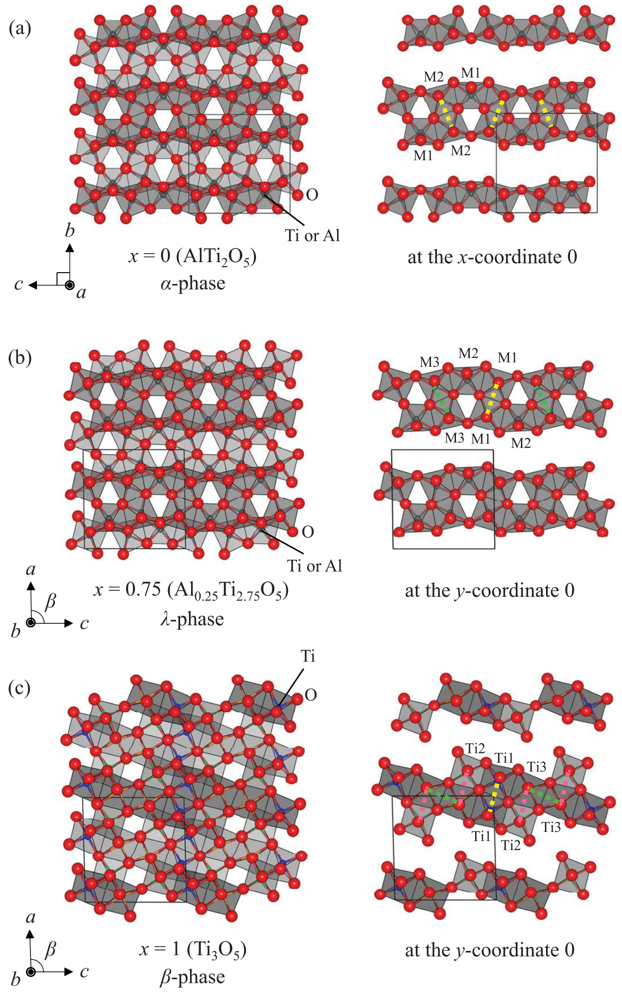

FIG. 1. Crystal structures at RT for (a) $AlTi_2O_5$ ($x = 0$) (α phase), (b) $Al_{0.25}Ti_{2.75}O_5$ ($x = 0.75$) (λ phase), and (c) Ti_3O_5 ($x = 1$) (β phase). In the left figure of (a), the octahedra with dark and light colors are at the x coordinates 0 and 1/4, respectively. The right figure of (a) extracts the structure at the x-coordinate 0 to make it easy to see. Similarly, the octahedra with dark and light colors in the left figures of (b) and (c) are at the y-coordinates 0 and 1/4, respectively, and the right figures of (b) and (c) extract the structures at the y-coordinate 0. The difference in color intensity at the same y coordinate of (c) shows the difference in valences of Ti ions in the center of a TiO_6 octahedron, which was deduced from the bond-valence sum. The valences of Ti ions of dark-color octahedra (Ti1 and Ti3) are close to 3, and those of light-color octahedra (Ti2) are close to 4. The dotted lines in the right figures of (a)–(c) represent the short Ti-Ti bonds.

random-phase approximation for a tight-binding model of nonrandom $AlTi_2O_5$ constructed from first principles. This CDW state is similar to the low-T phase of Ti_4O_7.

In this paper, we report the structural, magnetic, transport, and high-T thermoelectric (TE) properties of single crystals of the $AlTi_2O_5$-Ti_3O_5 mixed compound system ($Al_{1-x}Ti_{2+x}O_5$ for $0 \leqslant x \leqslant 1$) grown using a floating zone. We have found that the Al substitution suppresses the β phase at RT and consecutively induces the λ and α phases as shown in Fig. 1, similar to the substitution [12,13] of Fe and Mg at Ti sites in Ti_3O_5. Thus, the bulk $Al_{1-x}Ti_{2+x}O_5$ crystals for $0.5 < x \leqslant 0.8$ are in the pure λ phase at RT. Magnetization measurements reveal a lower number of Ti^{3+} ions than the formal number. This implies a correlation of spin-singlet Ti^{3+}-Ti^{3+} dimers coupled with the lattice even in the α and λ phases. The state in these phases is more conductive as x increases because the disorder is suppressed by the decrease in magnetic unpaired Ti^{3+} and nonmagnetic Al^{3+} ions. The decrease in the unpaired Ti^{3+} ions is due to the promoted correlation of some spin-singlet dimers with increasing x. Such a correlation of spin-singlet dimers may give rise to a high Seebeck coefficient in the conductive state, resulting in a large TE power factor (PF) at high T comparable to that in good n-type TE Ti oxides [14–16].

II. EXPERIMENTAL PROCEDURE

Single crystals of $Al_{1-x}Ti_{2+x}O_5$ were grown using a floating zone in an Ar gas flow containing 7% H_2 gas. The seed materials were prepared by sintering the mixed starting materials of Al_2O_3 (99.99% purity, Kojundo Co.), TiO_2 (99.99% purity, Kojundo Co.), and Ti_2O_3 (99.9% purity, Kojundo Co.) in air at 1000 °C for about 10 h in a muffle furnace. Powder x-ray diffraction (XRD) measurements of the obtained crystals with Cu $K\alpha$ radiation indicated no impurity phase. The structural parameters were obtained via Rietveld analysis of the powder XRD profiles as described in Sec. III A. According to the x-ray and neutron-scattering Laue photographs (some of which are shown in Fig. S1 of the Supplemental Material [17]), the obtained crystals having facets on the sides were nearly monocrystalline.

A Quantum Design magnetic property measurement system was used to measure the T dependence of the magnetic susceptibility $\chi = M/H$ in a magnetic field of 0.5 T and the magnetic-field dependence of magnetization M in a field from -5 to $+5$ T. The resistivity ρ at T below RT was measured with a four-probe method using a cryostat, whereas ρ and the Seebeck coefficient S were measured from RT to about 1000 K with a four-probe method using an Advance RIKO ZEM-3 high-T TE measurement system. Some ρ-T curves showed discontinuities around RT because we changed the measurement system. Although we can correct to make the data connect smoothly, we have not in order to eliminate arbitrariness from deriving the TE PF at high T. Furthermore, high-T data are absent for $x > 0.85$ because the crystals for $x > 0.85$ were so brittle and fragile that a large crystal could not be prepared for high T. ρ under high pressure was measured with a four-probe method using a cubic-anvil apparatus [18] providing homogeneous compression up to the maximum pressure of 20 GPa in this paper. The measurements for M, ρ, and S were performed along the crystal growth directions except for the ρ measurements under high pressures; ρ under high pressures was measured perpendicularly to the growth direction. As shown in Figs. S2 and S3 in the Supplemental Material [17], there was no large anisotropy in either χ or ρ in the α and λ phases. Because the observed slight differences between data recorded along each axis were comparable to the experimental errors, the observed distinct changes in physical properties with x in the α and λ phases were largely dominated by the changes in composition.

III. RESULTS AND DISCUSSION

A. Structural properties

Figure 2 shows the powder XRD profiles at RT of the $Al_{1-x}Ti_{2+x}O_5$ crystals with (a) $x = 0$ ($AlTi_2O_5$, α phase), (b) $x = 0.75$ (λ phase), (c) $x = 0.85$ (λ-β coexistent phase), and (d) $x = 1$ (Ti_3O_5, β phase) together with the results of the Rietveld refinement using RIETAN-FP [19]. There is clearly no impurity phase in any crystal, and the Rietveld refinement reproduces all Bragg peak positions for all compositions with the simplified models for α, λ, and β phases. Figure 3 and Tables S.I–S.VI of the Supplemental Material [17] show the detailed results of the Rietveld refinement of the powder XRD profiles, and Fig. 1 shows the structures of $x = 0$ (α phase), $x = 0.75$ (λ phase), and $x = 1$ (β phase) constructed using VESTA [20]. For $AlTi_2O_5$ [11], fitting a model with a random distribution of Al and Ti ions at the M1 and M2 sites [shown in Fig. 1(a)] is known to be better than using a model with a selective arrangement, such as placing Al ions at the M1 sites and Ti ions at the M2 sites. Hence, to exclude arbitrariness and simplify the model, this paper uses a random distribution of Al^{3+}, Ti^{3+}, and Ti^{4+} ions at each site for the refinements for all compositions, although there may be a better model with site selectivity.

According to the Rietveld analysis, the compounds for $0 \leqslant x \leqslant 0.5$ have an orthorhombic structure with space-group $Cmcm$ (α phase) at RT as shown in Fig. 2(a), which is the same structure as that reported for $AlTi_2O_5$ [11] and the high-T phase of Ti_3O_5 [1,2,4]. We found that the compounds for $0.5 < x \leqslant 0.8$ have a monoclinic structure with space-group $C2/m$ (λ phase) at RT as shown in Fig. 2(b), which is the same structure as those of the intermediate phase of Ti_3O_5 [4] and the Ti_3O_5 nanocrystal at RT [5]. Compounds for $0.9 < x \leqslant 1$ have another monoclinic structure with space-group $C2/m$ (β phase) as shown in Fig. 2(d), which is the same as that reported for the low-T β phase of Ti_3O_5 [1,2]. The boundary between the λ and the β phases is at $x \sim 0.9$, and the λ and β phases coexist near the boundary ($0.8 < x \leqslant 0.9$) as shown in Fig. 2(c). The upper bars under the profiles show the Bragg peak positions of the λ phase, and the lower bars indicate those of the β phase.

Figure 3 shows the x dependences of the lattice parameters and the volume fractions of the λ and β phases near the phase boundary $x \sim 0.9$. In Fig. 1, the lattice constant along the a and b axes in the α phase correspond to those along the b and a axes in the λ and β phases, respectively. As shown in Figs. 3(a)–3(c) and 3(e), all lattice constants and the unit-cell volume V linearly increase with increasing x up to the λ phase. There is no discontinuous change in lattice constants at the transition between the α and the λ phases because there is no significant crystal deformation at the transition in Figs. 1(a) and 1(b). Furthermore, the angle (β angle) between the a and the c axes only changes from 90° in Fig. 3(d). However, all lattice parameters and the volume of the unit cell discontinuously change at the transition from the λ phase to the β phase. These behaviors are similar to the T dependences of the structural parameters in Ti_3O_5 [4] where the successive structural phase transition from the α phase to the β phase through the λ phase occurs as T decreases.

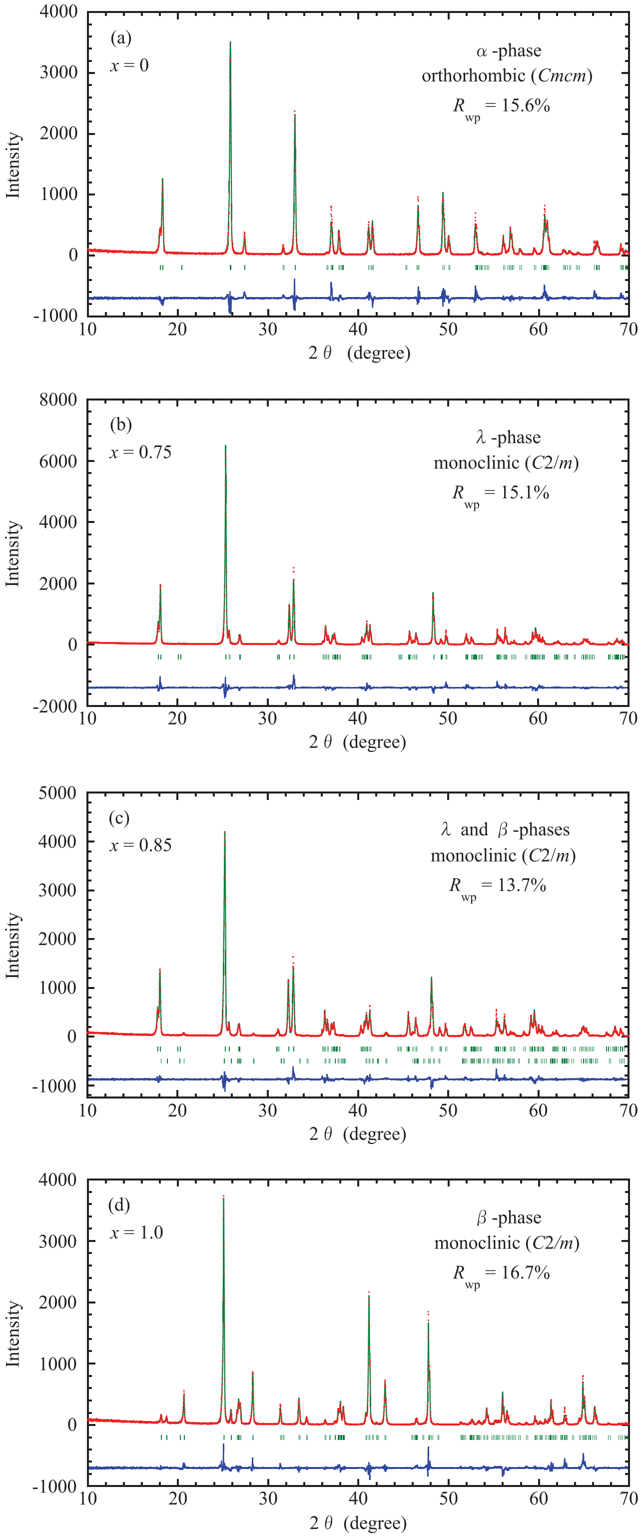

FIG. 2. Powder x-ray diffraction profiles of $Al_{1-x}Ti_{2+x}O_5$ for (a) $x = 0$ ($AlTi_2O_5$), (b) $x = 0.75$, (c) $x = 0.85$, and (d) $x = 1$ (Ti_3O_5). Filled circles and solid lines show the observed profiles and profiles calculated via Rietveld analysis, respectively, whereas the bars and the line under the observed and calculated profiles show the expected Bragg peak positions and the difference between the observed and the calculated data, respectively. The obtained crystal parameters are summarized in Fig. 3 and Tables S.I– S.VI of the Supplemental Material [17].

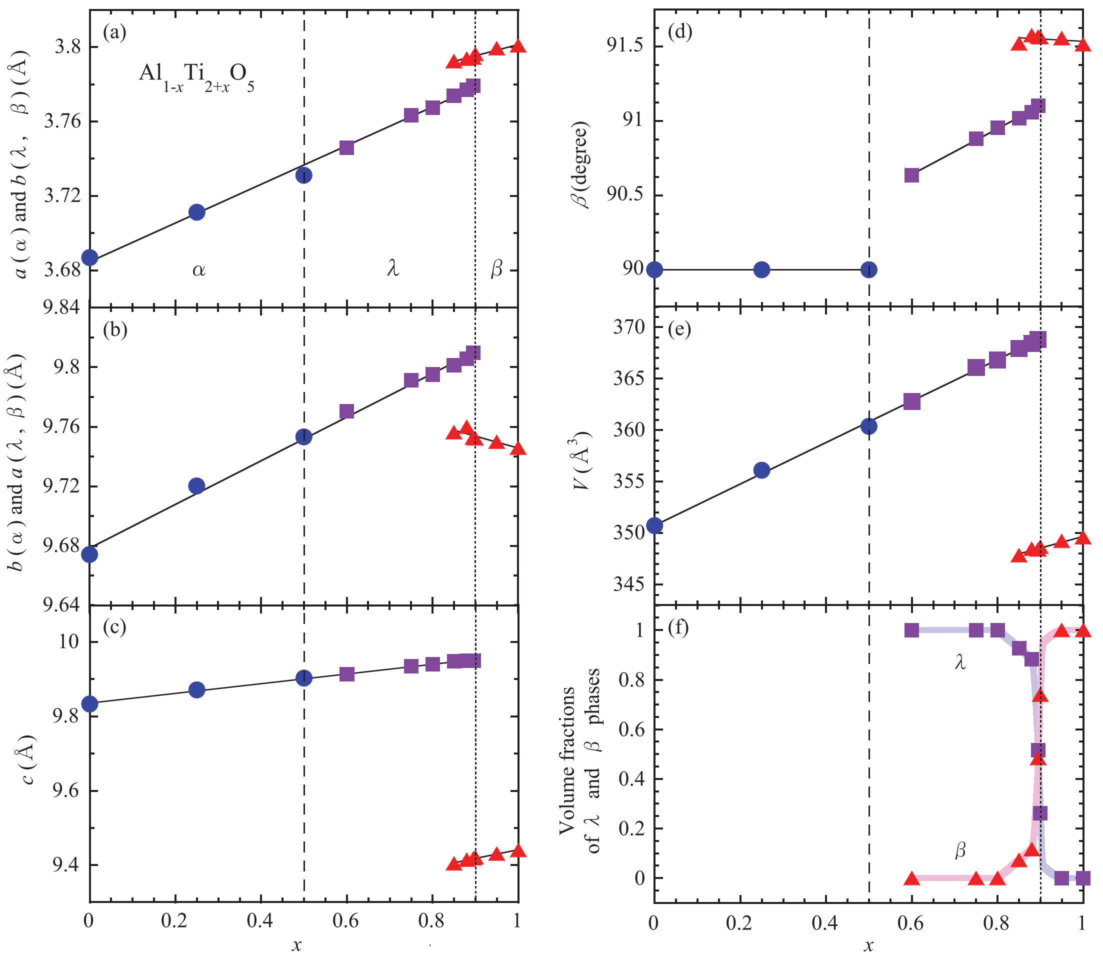

FIG. 3. Crystal parameters at RT obtained via Rietveld analysis. (a)–(c) show x dependences of lattice constants of $Al_{1-x}Ti_{2+x}O_5$ along the (a) a axis in the α phase ($0 \leqslant x \leqslant 0.5$) and b axis in the λ and β phases ($0.5 < x \leqslant 1$), (b) b axis in the α phase and a axis in the λ and β phases, and (c) c axis. (d)–(f) show the (d) angle between the a axis and the c axis (β angle), (e) unit-cell volume V, and (f) volume fractions of λ and β phases near the phase boundary ($x \sim 0.9$). The solid and thick solid lines are guides for the eyes. The vertical dashed line at $x = 0.5$ shows the boundary between the α and the λ phases at RT, whereas the vertical dotted line at $x = 0.9$ shows the boundary between the λ and the β phases at RT.

However, as shown in Fig. 3(f), the λ phase is a major phase, and the β phase is a minor phase at RT below $x \sim 0.9$, and vice-versa above $x \sim 0.9$. Hence, $x \sim 0.9$ is regarded as the phase boundary between the λ and the β phases. Figure 4 shows the rough phase diagram of $Al_{1-x}Ti_{2+x}O_5$ determined from the powder XRD measurements at RT together with the measurements of M and high-T S discussed later.

The Ti1-Ti1 and Ti3-Ti3 bonds in the low-T β phase of Ti_3O_5 are represented by the yellow and green dotted lines in the right figure of Fig. 1(c). It has been reported that these distances between Ti^{3+} ions are short, and their localized spins are antiferromagnetically coupled to form charge-ordered spin-singlet Ti^{3+}-Ti^{3+} dimers [1,2,4,21]. Our powder XRD results largely reproduce the previous bond lengths, judging from those in Table S.VI of the Supplemental Material [17]. The ion valences [22] at the Ti1, Ti2, and Ti3 sites deduced from the Ti-O bond lengths in Table S.VI of the Supplemental Material [17] are 3.044, 3.907, and 3.408, respectively, suggesting some charge ordering represented by the color gradation of the TiO_6 octahedra in the right figure of Fig. 1(c). Furthermore, the Ti1-Ti1 distance (2.655 Å), Ti2-Ti3 distance (2.834 Å), and Ti3-Ti3 distance (2.844 Å) represented by the thick dotted lines in the right figure of Fig. 1(c) are considerably short. These are less than the Ti-Ti distances in the α-Ti metal (2.93 Å) and rutile TiO_2 (2.96 Å), suggesting the formation of Ti^{3+}-Ti^{3+} pairs. Although there are small differences between the previous results and our results due to our simplified fitting model or to the measurement accuracy, the overall features indicating some charge order state are consistent.

It is interesting that there are also short Ti^{3+}-Ti^{3+} distances, suggesting some correlation of Ti^{3}-Ti^{3+} dimers in both the α and the λ phases. As shown in Tables S.IV and S.V of the Supplemental Material [17], the M2-M2 distance in the α phase ($0 \leqslant x \leqslant 0.5$) and the M1-M1 distance in the λ phase ($0.5 < x < 0.9$) are 2.83–2.89 and 2.69–2.81 Å, respectively. The M1–M3 sites are those at which the virtual chemical species with compositions $\frac{1-x}{3}Al^{3+}$, $\frac{1+x}{3}Ti^{3+}$, and $\frac{1}{3}Ti^{4+}$ are placed in our random-distribution model. These deduced lengths are also less than the distances in the α-Ti metal and rutile TiO_2.

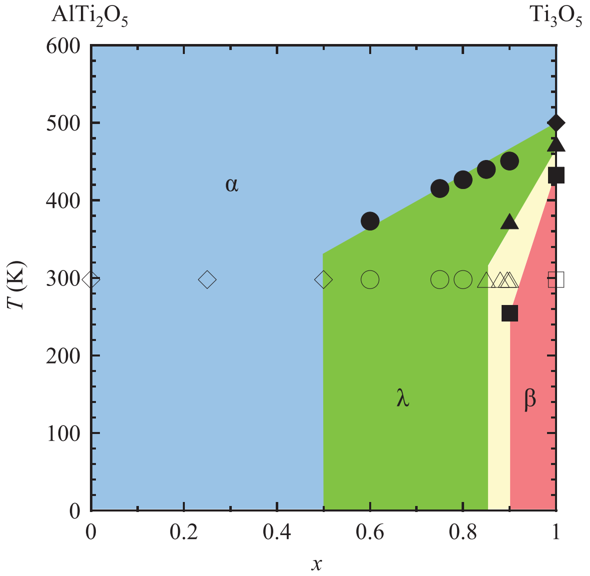

FIG. 4. Phase diagram of $Al_{1-x}Ti_{2+x}O_5$ determined by the measurements of powder XRD, M, and S. The filled circles show the kink temperatures in the T dependences of S, and the filled triangles and filled squares show the transition temperatures deduced from the measurements of M on heating and on cooling, respectively. The filled diamond at $x = 1$ (Ti_3O_5) shows the temperature of the structural transition between the high-T α phase and the middle λ phase determined by the kink in the χ-T curve (not shown). The open diamonds, circles, triangles, and squares show the measurement temperatures of the powder XRD, revealing the α phase, λ phase, λ-β coexistent phase, and β phase, respectively.

However, as shown in Tables S.IV– S.VI of the Supplemental Material [17] the differences between the average M1-O and M2-O distances in the α phase are smaller than those among the average Ti1-O (or Ti3-O) and Ti2-O distances in the β phase of Ti_3O_5, and the differences among the M1-O–M3-O distances in the λ phase are also smaller than those in the β phase of Ti_3O_5. In addition to the smaller differences between the distances to O ions, the shortest Ti-Ti distance increases as the amount of Al increases with decreasing x, although the ionic radius of the Al^{3+} ion is smaller than those of Ti^{3+} and Ti^{4+} ions. Although some correlation of Ti^{3+}-Ti^{3+} dimers seems to remain in the α and λ phases, these results imply that Ti^{3+} ions are distributed more homogeneously in these phases than in the β phase. This may relate to the better conductivity in the α and λ phases than in the β phase as discussed in Sec. III C.

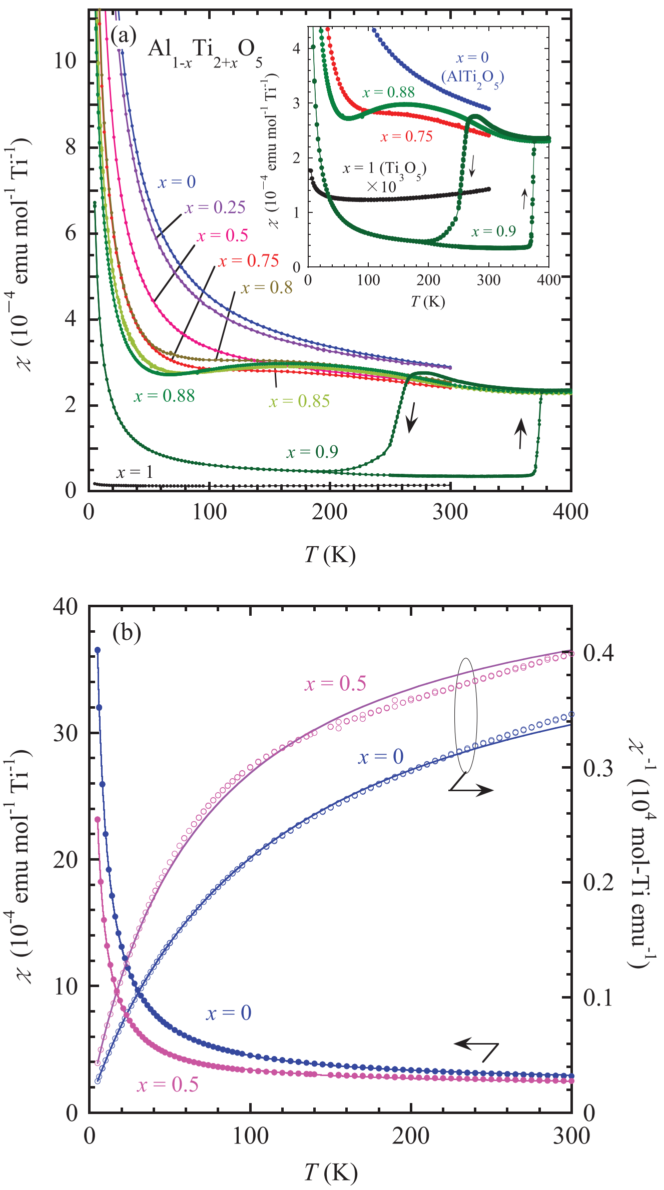

FIG. 5. χ-T curves of $Al_{1-x}Ti_{2+x}O_5$ for $0 \leqslant x \leqslant 1$ at $H = 0.5$ T. The inset shows the magnifications of χ-T curves for $x = 0$, 0.75, 0.88, 0.99, and 1. (b) χ-T and χ^{-1}-T curves for $x = 0$ and 0.5 with the results of fitting to the Curie-Weiss relation $\chi = M/H = C/(T - \theta_{\rm CW}) + \chi_0$, where $\theta_{\rm CW}$ is the Curie-Weiss temperature and χ_0 is a constant. The solid lines show the fitting results for both compounds and the deduced $\theta_{\rm CW}$ and χ_0 are summarized in Table I.

B. Magnetic properties

Figure 5(a) shows the T dependence of the magnetic susceptibility $\chi = M/H$ of $Al_{1-x}Ti_{2+x}O_5$ for $0 \leqslant x \leqslant 1$. χ monotonically decreases as x increases to 0.5. As shown in Fig. 5(b), χ for the α-phase compounds ($0 \leqslant x \leqslant 0.5$) well obeys the Curie-Weiss relation with the constant component χ_0: $\chi = M/H = \frac{C}{T-\theta_{\rm CW}} + \chi_0$. If the Curie-Weiss components are assumed to come from the spin magnetic moment of the Ti^{3+} ($3d^1$, spin 1/2) ion, we can estimate the number of Ti^{3+} [$n(Ti^{3+})$] ions from the obtained Curie constant $C = n(Ti^{3+})S(S+1)g^2\mu_B^2/(3k_B)$, where S and g, respectively, are the spin quantum number and the g factor of a $3d$ electron ($g = 2$). The solid squares in Fig. 7 show the number of Ti^{3+} ions per Ti atom [$n(Ti^{3+})/n_0(Ti^{3+})$] against the number [$n_0(Ti^{3+})$] calculated from the formal valence of Ti ions. It is clear that $n(Ti^{3+})$ is much smaller than $n_0(Ti^{3+})$ even for $AlTi_2O_5$. The number $n(Ti^{3+})$ further decreases with increasing x, which is qualitatively different from the x dependence of $n_0(Ti^{3+})$, monotonically increasing with x according to $(1+x)/(2+x)$. Most of the Ti^{3+} spins disappear even in the α phase.

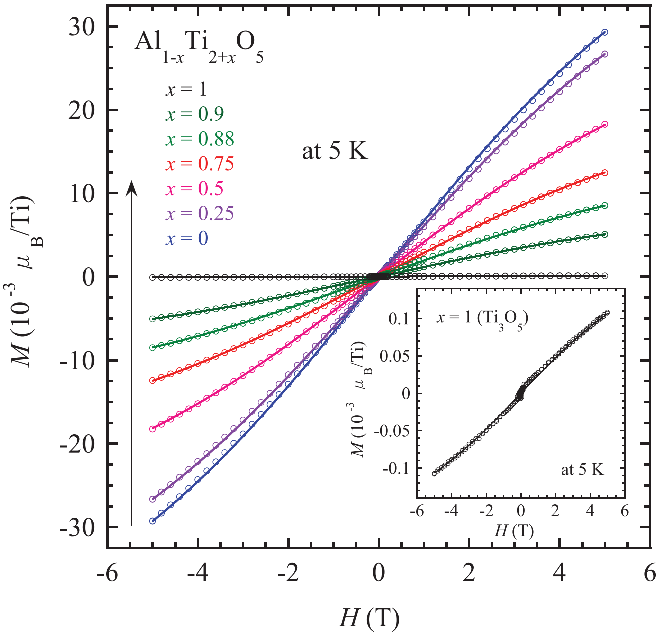

FIG. 6. M-H curves of $Al_{1-x}Ti_{2+x}O_5$ for $x = 0$, 0.25, 0.5, 0.75, 0.88, 0.9, and 1 at 5 K. The solid lines are the calculated curves. The inset shows the magnification of the result for $x = 1$ (Ti_3O_5). The solid line in the inset is also the calculated curve. By manually varying $n(Ti^{3+})$ in these analyses, we adjust the calculated line to the observed data (open circles).

Table I gives θ_{CW} and χ_0 for $x = 0$, 0.25, and 0.5 deduced from fitting to the Curie-Weiss relation. The small absolute values of θ_{CW} imply that this system is nearly an isolated spin system. We can attribute χ_0 to the T-independent component of the high-T α phase of Ti_3O_5 [2,4], which is mainly due to contributions of diamagnetism from the ion core, Landau diamagnetism, and Van Vleck paramagnetism because judging from the insulating behaviors of ρ discussed later, the contribution of Pauli paramagnetism should be small.

As x increases beyond 0.5, the λ phase appears at RT (Fig. 4) and the χ-T curve nonmonotonically changes. The inset of Fig. 5(a) magnifies the χ-T curves for $x = 0$, 0.75, 0.88, and 1 so that they are easy to view. The χ at low T is gradually suppressed as x increases, whereas χ around 150 K is slightly enhanced as x gets closer to the boundary between the and β phases, $x \sim 0.9$. This unique χ-T curve near the phase boundary is similar to that observed for the λ phase of the Ti_3O_5 nanocrystal [5].

As shown in Fig. 5(a), χ suddenly drops at $x = 0.9$ around RT as T decreases, accompanying a large hysteresis whose transition temperature is about 255 K on cooling and about 373 K on heating. This indicates a first-order magnetic transition to a nearly nonmagnetic state at low T. This first-order magnetic transition is perhaps the same as that observed in Ti_3O_5 where the structural and magnetic phase transitions are reported to simultaneously occur at about 440 K on cooling and at about 460 K on heating [3]. This is nearly reproduced by our Ti_3O_5 crystal, whose transition temperature is about 433 K on cooling and about 473 K on heating (not shown). The transition temperature largely decreases, and the temperature width of the hysteresis becomes wider as the nonmagnetic Al doping increases with decreasing x, and lastly vanishes if the Al doping exceeds 10% ($x < 0.9$).

TABLE I. θ_{CW} and χ_0 for $x = 0$, 0.25, and 0.5 deduced from the fitting of χ to the Curie-Weiss relation shown in Fig. 5(b).

x	θ_{CW} (K)	χ_0 (10^{-4} emu mol^{-1} Ti^{-1})
0	−2.00	2.17
0.25	−1.94	2.17
0.5	−1.52	2.03

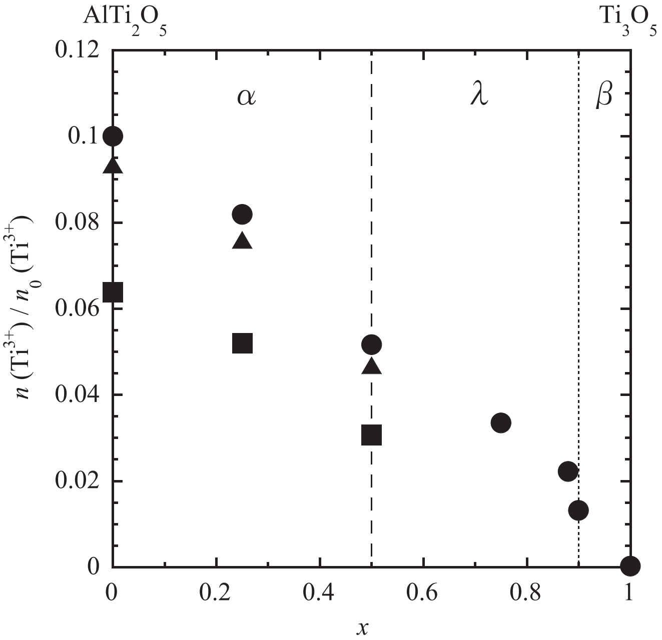

FIG. 7. Number of Ti^{3+} ions per Ti atom [$n(Ti^{3+})$] deduced from the χ-T and M-H curves against this number calculated from the formal valence of Ti ions [$n_0(Ti^{3+}) = (1 + x)/(2 + x)$]. Filled squares are the ratios deduced from the Curie-Weiss constant determined by fitting the χ-T curves, and filled circles and filled triangles are those deduced from the M-H curves without and with the H-linear contributions to M, respectively.

Figure 6 shows the M-H curves at 5 K for $x = 0$, 0.25, 0.5, 0.75, 0.88, 0.9, and 1, where the solid lines are the calculated M values. Except for $x = 1$ (Ti_3O_5), all M-H curves are largely explained by the simple model,

$$M(H) = n(\mathrm{Ti}^{3+}) g S \mu_B B_S(x), \qquad (1)$$

where S is the spin quantum number and $B_S(x)$ is the Brillouin function with the variable x ($\equiv g S \mu_B H / k_B T$). As in the case of the α phase, the magnetism in the λ phase is assumed to come from the residual isolated spin 1/2 of Ti^{3+} ions. We neglected the antiferromagnetic molecular field and varied $n(Ti^{3+})$ as a parameter to fit the calculation to the data. Slightly better fitting results can be obtained using a model with an H-linear component ($\chi_0 H$); however, except for $0 \leqslant x \leqslant 0.5$, we cannot experimentally determine χ_0 for $0.5 < x \leqslant 1$ from the χ-T curves at 0.5 T.

Although there is a tiny step around $H = 0$ in the M-H curve of Ti_3O_5 in the inset of Fig. 6, the above simple model was used to roughly estimate the isolated spin in the low-T β phase of Ti_3O_5. The solid line in the inset of Fig. 6 is the fitting result. The estimated $n(Ti^{3+})$ for low-T β-Ti_3O_5 is quite small and negligible compared with that for the other compositions, which is consistent with the formation of nearly perfect charge-ordered spin-singlet dimers in the β phase of Ti_3O_5.

Figure 7 shows the relative number of Ti^{3+} ions $[n(Ti^{3+})/n_0(Ti^{3+})]$ for $0 \leqslant x \leqslant 1$ deduced from the M-H curves together with that for $0 \leqslant x \leqslant 0.5$ deduced from the χ-T curves (Curie constant C). The filled circles and filled triangles show $n(Ti^{3+})/n_0(Ti^{3+})$ deduced from fitting to the M-H curves with and without an H-linear component, respectively. It is clear that $n(Ti^{3+})/n_0(Ti^{3+})$ monotonically decreases with increasing x. There are small differences between the $n(Ti^{3+})/n_0(Ti^{3+})$ values with and without an H-linear component and the $n(Ti^{3+})/n_0(Ti^{3+})$ values from the M-H curve are about 1.5 times those from the χ-T curves (the filled squares). However, these differences do not affect the qualitative change with x. The spins of Ti^{3+} ions in the α and λ phases gradually disappear as x gets closer to the phase boundary $x \sim 0.9$, which indicates that the correlation of nonmagnetic spin-singlet Ti^{3+}-Ti^{3+} dimers develops with increasing x.

As discussed in Sec. III A, the M2-M2 distance in the α phase and the M1-M1 distance in the λ phase at RT are less than those in the α-Ti metal and in rutile TiO_2. This short Ti-Ti distance decreases with increasing x as summarized in Tables S.IV– S.VI of the Supplemental Material [17]. In addition to the disappearance of most Ti^{3+} ion spins in these phases, such changes in interatomic bond lengths indicate developing correlation of spin-singlet dimers in the α and λ phases with increasing x.

In the β phase, the Ti^{3+} and Ti^{4+} ion orders and almost all Ti^{3+} ions participate in forming static spin-singlet dimers, leading to the nonmagnetic state. However, in the α and λ phases, the nonmagnetic spin-singlet Ti^{3+}-Ti^{3+} dimers form only when the Ti^{3+} ions simultaneously occupy two neighboring M2 sites in the α phase or two neighboring M1 or M3 sites in the λ phase. The Ti^{3+} ions that do not participate in dimer formation are left as unpaired Ti^{3+} ions. As x increases, the formal valence of Ti ions decreases according to $(7+3x)/(2+x)$, and the Ti^{3+} ions increase in number. However, this increase in Ti^{3+} ions actually promotes the formation of the spin-singlet Ti^{3+}-Ti^{3+} dimers, resulting in the gradual disappearance of spin with increasing x.

C. Transport properties

1. *Resistivity*

According to previous first-principles calculations, the Fermi level (E_F) is located in the $3d$ t_{2g} band in both α-$AlTi_2O_5$ [11] and λ-Ti_3O_5 [5], revealing a metallic nature of these phases. Nevertheless, it has been reported that $AlTi_2O_5$ polycrystals show insulating behavior [11]. Tohyama *et al.* proposed that such insulating behavior might be due to a nesting-driving CDW order similar to that of the low-T phase of Ti_4O_7 [8,23]. This would originate from a pseudo-two-dimensional (2D) electronic structure reflecting 2D Ti layers stacked along the c axis.

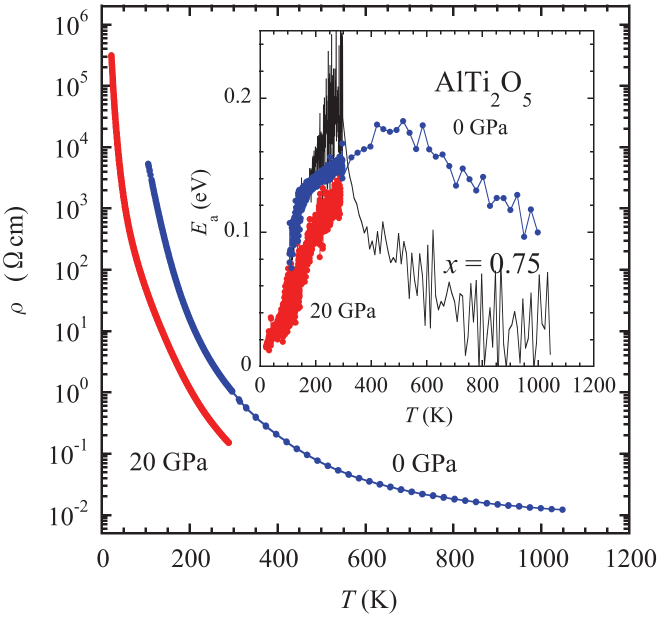

FIG. 8. ρ-T curves of $AlTi_2O_5$ ($x = 0$) at ambient pressure (0 GPa) below 1050 K and at 20 GPa below RT. The inset shows the local activation energy ($E_a = d \ln \rho / dT^{-1}$) deduced from the ρ-T curves. The closed circles show E_a for $x = 0$ without and with applying pressures, and the line shows that for $x = 0.75$.

The resistivity ρ of our $AlTi_2O_5$ crystal also shows insulating behavior in Fig. 8, but there is no clear sign of a phase transition to a CDW state from about 100 K to about 1000 K. The inset of Fig. 8 shows that the local activation energy E_a deduced from the ρ-T curve is less than 0.2 eV throughout the T region, which is close to an energy gap in λ-Ti_4O_7 [9,10] and in some CDW materials [23]. Hydrostatic pressure may be able to suppress such a small energy gap and make the compound metallic as observed in Ti_4O_7 [24]. However, as shown in Fig. 8, the $AlTi_2O_5$ crystal does not become metallic even under pressures up to 20 GPa, although ρ and E_a largely decrease at low T.

Next, Fig. 9 shows the ρ-T curves for all compounds ($0 \leqslant x \leqslant 1$), and Fig. 10 shows the x dependences of ρ at 290 and 1000 K. Although ρ in Fig. 9 shows insulating behavior for all compounds, it monotonically decreases as x increases to 0.75. In Fig. 10, ρ at around $x \sim 0.75$ has the smallest values of about 2×10^{-2} Ω cm at RT and about 3×10^{-3} Ω cm at 1000 K among the compositions we investigated. ρ at RT for $x = 0.75$ is lower than that observed at 20 GPa for $AlTi_2O_5$. As shown in the insets of Figs. 8 and 9, E_a has a peak and largely decreases with an increase in T for $0 \leqslant x < 0.9$. Furthermore, the peak temperature lowers and E_a at 1000 K decreases with an increase in x. Such a feature suggests that some crossover from a nearly localized state to a nearly itinerant state occurs with increases in T and x.

According to the first-principles calculation of λ-Ti_3O_5 performed by Ohkoshi *et al.* [5], the band of the Ti^{3+}-Ti^{3+} dimer generated by the σ-type bonding of d_{xy} orbitals on M1 is located at -0.58 eV from E_F in the λ phase. This is connected with the band near the Fermi energy generated by the π stacking between the d_{xy} orbital on M2 and that on

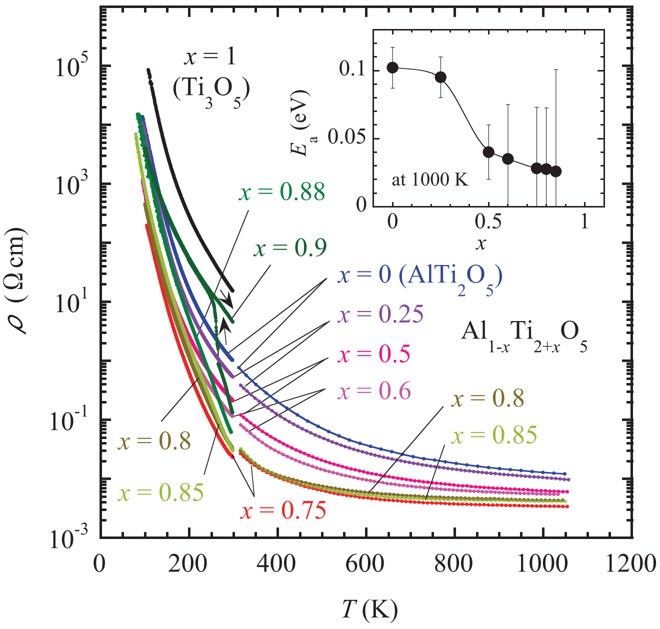

FIG. 9. ρ-T curves of $Al_{1-x}Ti_{2+x}O_5$ for $0 \leqslant x \leqslant 1$. The inset shows the x dependence of E_a at 1000 K.

M3. Al ions at the M1 sites should then disturb the dimer formation and produce the unpaired Ti^{3+} ions that become magnetic impurities, whereas the Al ions should themselves become nonmagnetic impurities on the electron conduction path. This means the disorder in $Al_{1-x}Ti_{2+x}O_5$ is induced by the magnetic and nonmagnetic impurities produced by Al substitutions, which results in the observed x dependences of ρ because the carrier concentration does not significantly change with x as discussed in the next section. We might better regard $AlTi_2O_5$ as a disordered spin-singlet Ti^{3+}-Ti^{3+} dimer compound because the electronic structure of the α phase is not expected to significantly differ from that of the λ phase.

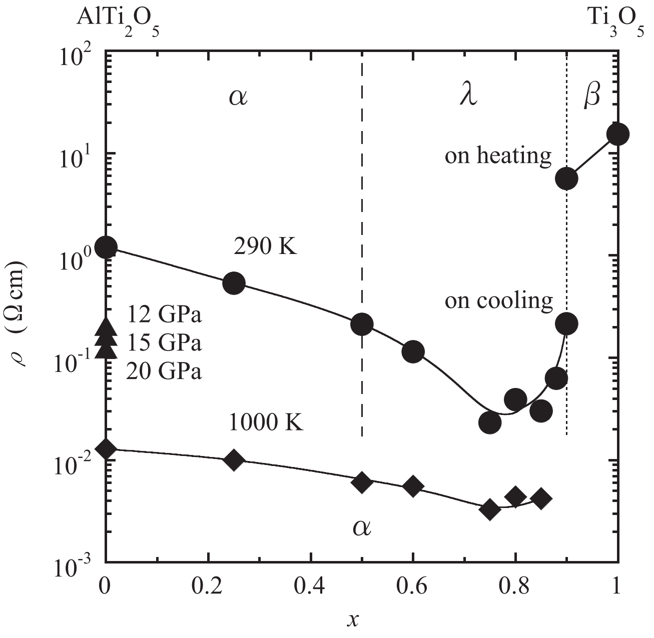

FIG. 10. x dependences of ρ of $Al_{1-x}Ti_{2+x}O_5$ at 290 and 1000 K. The closed circles and closed diamonds show ρ at 290 and 1000 K, respectively. The closed triangles show ρ of $AlTi_2O_5$ at 290 K at 12, 15, and 20 GPa. The solid lines are guides for the eyes. The vertical dashed line at $x = 0.5$ shows the boundary between the α and the λ phases at RT, whereas the vertical dotted line at $x = 0.9$ shows the boundary between the λ and the β phases at RT.

However, ρ increases as x increases from about 0.8 to about 0.9 owing to the appearance of the β phase with lower electric conduction as a secondary phase. The ρ-T curve for $x = 0.9$ in Fig. 9 shows a history corresponding to the hysteresis of the χ-T curve, which results from the first-order magnetic transition accompanying the first-order structural phase transition between the λ and the β phases. The ρ value in the β phase is higher than values in the α and λ phases and further increases as x increases to 1. This is perhaps due to the stabilization of the charge-ordered spin-singlet dimer. E_a values for Ti_3O_5 estimated from the ρ-T curve are 0.1–0.2 eV, which are almost consistent with the band gaps estimated [5] from theory and from the optical reflection spectrum.

As discussed in the previous sections, the correlation of the spin-singlet dimer is well developed in the conductive region around $x = 0.75$ near the phase boundary $x \sim 0.9$. This is evidenced by the disappearance of most of the spins. The electron hopping between the Ti sites in such a regime may make the spin-singlet dimer dynamic, such as for a resonating valence bond state [25] or an intermediate state of Ti_4O_7 [9]. The structural phase transition between the β and the λ phases may accompany the transition between the solid and the liquid dimer states, resulting in fluctuation of the spin-singlet dimer and leading to the critical enhancement of χ at around 150 K near the phase boundary ($x \sim 0.9$) in Fig. 5(a).

2. *Seebeck coefficient in the high-T α phase*

As discussed so far, the correlation of spin-singlet dimers develops even in the α and λ phases where the $Al_{1-x}Ti_{2+x}O_5$ system shows relatively good electric conductivities at high T. The compound for $x = 0.75$ nearly shows band conduction at high T, and its electric conductivity reaches $\sim 3 \times 10^2$ S cm^{-1} at 1000 K. This itinerant correlated state in the high-T region may show a good TE response, such as those of some Co oxides [26] and Ti oxides [16].

Figure 11(a) shows the T dependences of the Seebeck coefficient S above RT. The kinks are at 400–450 K in the S-T curves for $x > 0.5$. Judging from the previous report on the high-T phases of Ti_3O_5 [4], the kink temperatures correspond to the critical temperature of the second-order phase transition between the α and the λ phases, which we used to draw the rough phase diagram in Fig. 4. All $Al_{1-x}Ti_{2+x}O_5$ compounds in Fig. 4 are then in the α phase at high T.

The Seebeck coefficient in the high-T α phase roughly consists of two components: a T-linear component $(dS/dT)_\alpha T$ and a constant component S_0. Two similar components in the S-T curves have been reported for some disordered electron systems [27,28]. We now suppose a disordered electron system with a Fermi level (E_F) in a hopping conduction regime far below a critical energy (E_c) ($k_BT \ll E_c - E_F$). Following Cutler and Mott [27], we substitute the conductivitylike function $\sigma(E) = e\mu(E_F)N(E_F)k_BT$ into the Mott formula to express S

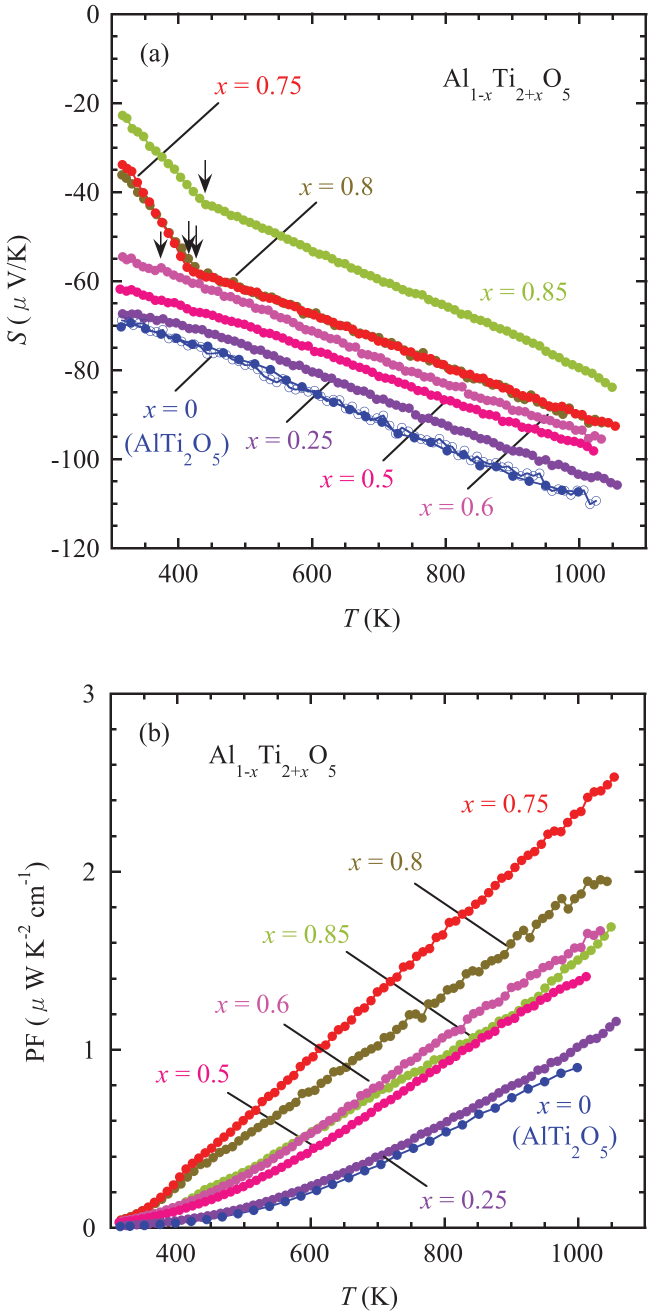

FIG. 11. T dependences of (a) S and (b) PF of $Al_{1-x}Ti_{2+x}O_5$ for $0 \leqslant x \leqslant 1$. The arrows show the kink temperatures indicating the structural phase transitions between the α and the λ phases. The open circles in (a) show the result for another $AlTi_2O_5$ crystal.

in this system as

$$S = -\frac{\pi^2 k_B}{3e}\left(k_B T \frac{\partial \ln(\mu_0 N)}{\partial E} - \frac{\partial E_a}{\partial E}\right)_{E=E_F}, \qquad (2)$$

where $\mu(E) = \mu_0(E)\exp[-E_a(E)/k_B T]$ is an activated mobility, $N(E)$ is the density of states, and E_c is the critical energy separating the localized states from the unlocalized ones. In this $Al_{1-x}Ti_{2+x}O_5$ system, the formation of spin-singlet Ti^{3+}-Ti^{3+} dimers or trap centers caused by nonmagnetic Al ions, unpaired isolated Ti ions, or lattice defects should disturb the conduction of the d electrons. This should induce hopping conduction of the d electrons at low T, whereas the metallic nature should recover at high T owing to the thermal activation of the d electrons trapped at the sites of the spin-singlet dimers or at the trap centers. As discussed in the previous section, the results of ρ and E_a also indicate a crossover from the nearly localized state to the nearly itinerant state with an increase in T.

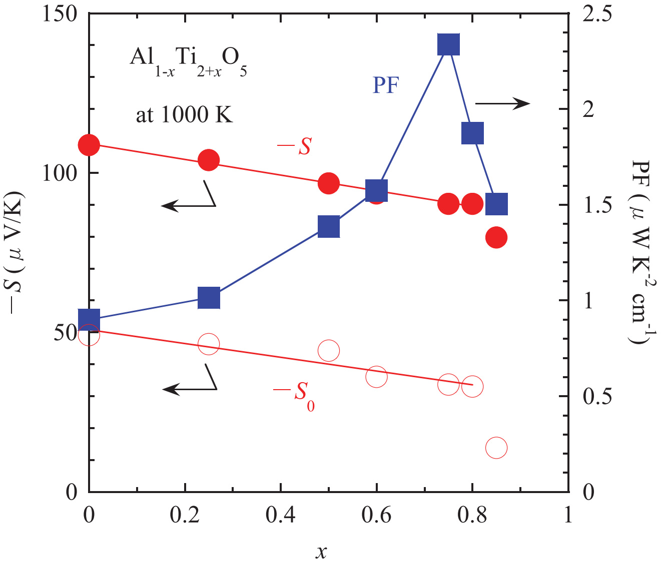

FIG. 12. x dependences of S, S_0, and PF at 1000 K for $Al_{1-x}Ti_{2+x}O_5$.

Figure 12 shows the x dependences of the measured S, its constant component S_0 estimated from the T-linear fitting, and the TE PF at 1000 K. The absolute value of S_0 almost linearly decreases as the Ti ion number (x) increases and ρ decreases, except for $x = 0.85$ where the λ and β phases coexist. This reduction of $|S_0|$ with increasing electric conductivity has been observed in other systems [27,28].

The behaviors of ρ and S might be explained by the increase in carrier concentration n_e with x, which increases E_F and brings it closer to E_c. The formal value of n_e deduced from the chemical formula certainly increases with increasing x. However, as the number of Al ions in the $Al_{1-x}Ti_{2+x}O_5$ system decreases with increasing x, the number of unpaired Ti^{3+} ions also decreases owing to the promoted formation of the spin-singlet Ti^{3+}-Ti^{3+} dimers as discussed before. In fact, the T-linear coefficient $(dS/dT)_\alpha$ deduced from the fitting in the high-T α phase is about −0.0600, −0.0570, −0.0525, −0.0583, −0.0565, and −0.0574 for $x = 0$, 0.25, 0.5, 0.6, 0.75, 0.8, and 0.85, respectively. When we assume the density of states is three dimensional, and μ_0 is independent of E, the T-linear coefficient is proportional to $-k_B^2/eE_F$ as for a metal. Assuming that the effective mass does not change with x, the carrier concentration per formula unit normalized by the concentration for $x = 0$ $[n_e(x)/n_e(0)]$ is estimated to be 1.080, 1.221, 1.044, 1.095, 1.067, and 0.884 for $x = 0.25$, 0.5, 0.6, 0.75, 0.8, and 0.85, respectively. The estimated $n_e(x)/n_e(0)$ values are smaller than values expected from the formal valences $(1 + x)$ even taking into account experimental errors. Furthermore, the difference becomes larger as the composition approaches the boundary between the λ and the β phases, $x \sim 0.9$.

The behaviors of ρ and S might also be consistently explained by the remarkable suppression of disorder with an increase in x. The decrease in the number of Al ions decreases the number of unpaired Ti^{3+} ions owing to the promoted formation of the dimers, which should remarkably suppress the disorder induced by these nonmagnetic and magnetic ions. As a result, even if n_e and E_F do not change, E_F can approach E_c owing to the decrease in E_c. Then, ρ dramatically decreases, and $|S_0|$ decreases without a large change in $(dS/dT)_\alpha$ with an increase in x.

The electric conductivity improves as T increases owing to the thermal activation of the carrier as discussed before, and $|S|$ linearly increases with T. Hence, the TE PF $\equiv S^2/\rho$ for all compounds increases as T increases in Fig. 11(b). Furthermore, Fig. 12 shows that the change in S with x at 1000 K originates almost entirely from the change in S_0, so the relatively high $|S|$ value of ~100 μV/K is kept at high T with x up to 0.8. The $x = 0.75$ compound has the lowest resistivity among the compounds we investigated with a low ρ value of $\sim 10^{-3}$ Ω cm that is almost T independent in the high-T α phase. This results in the highest TE PF of about 2.4 $\mu\mathrm{W\,K^{-2}\,cm^{-1}}$ at 1000 K as shown in Fig. 12. This value is about 1/10 times that of a good TE material.

We have discussed the correlations of the spin-singlet Ti^{3+}-Ti^{3+} dimers in the α and λ phases as well as in the β phase where the static charge-ordered spin-singlet Ti^{3+}-Ti^{3+} dimers are stable. The α and λ phases have much higher conductivities than the β phase not only because of the difference in structure, but also because the temperature and disorder moderately suppress the charge-ordered dimer. The itinerant carrier in such a correlated conductive phase often involves various interactions between the internal degrees of freedom, such as the charge, spin, orbital, and lattice, resulting in various exotic phenomena as observed in colossal magnetoresistive manganites [29]. In the $Al_{1-x}Ti_{2+x}O_5$ system, the electrons that become itinerant at high T should involve the correlation of the charge-ordered spin-singlet dimers coupled with the lattice. This may result in a good TE property due to an enhanced effective electron mass.

IV. SUMMARY

In this paper, we grew single crystals of the pseudobrookite $Al_{1-x}Ti_{2+x}O_5$ for $0 \leqslant x \leqslant 1$ and investigated structural, magnetic, transport, and TE properties along the growth direction. We found that the λ phase is stable at RT for $0.5 < x < 0.9$ and generated the rough phase diagram of $Al_{1-x}Ti_{2+x}O_5$ for $0 \leqslant x \leqslant 1$.

As for magnetic properties, we have found that the numbers of Ti^{3+} ions ($3d^1$, spin 1/2) deduced from the χ-T and M-H curves are much smaller than those expected from the formal valences, and these ions gradually disappear with increasing x. The results strongly indicate developing correlation of the spin-singlet Ti^{3+}-Ti^{3+} dimers even in the α and λ phases. Furthermore, we have found critical enhancement of magnetic susceptibility at around 150 K near the boundary between the λ and β phases, perhaps originating from fluctuation of charge-ordered spin-singlet dimers.

Although the resistivity ρ for all compositions shows insulating behavior from about 100 to about 1000 K, ρ in the α and λ phases is lower than that in the β phase where almost all Ti^{3+} ions participate in forming the charge-ordered spin-singlet Ti^{3+}-Ti^{3+} dimers. The resistivity for $0 \leqslant x < 0.9$ largely decreases with increasing x except near the boundary between the λ and the β phases ($x \sim 0.9$). A crossover from a nearly localized state to a nearly itinerant state seems to occur with increases in x and T. The increase in electric conductivity originates from the remarkable suppression of disorder due to the decrease in the numbers of nonmagnetic Al^{3+} and unpaired magnetic Ti^{3+} ions. This is consistent with the fact that the Seebeck coefficient has a T-linear component with a constant component, which is a characteristic of a disordered metal, and this constant component decreases with increasing x.

The $x = 0.75$ compound with the lowest resistivity among the compounds that we investigated has a relatively good TE power factor of about 2.4 $\mu\mathrm{W\,K^{-2}\,cm^{-1}}$ at 1000 K. The correlation of the spin-singlet dimers spreads in the conductive α and λ phases and may result in their large negative Seebeck coefficients, leading to a good TE property in the high-T α phase.

ACKNOWLEDGMENTS

We thank Prof. D. I. Khomskiĭ for helpful discussions. This work was supported by the Japan Society for the Promotion of Science (KAKENHI Grant No. 18K03543) and was partly carried out at the Joint Research Center for Environmentally Conscious Technologies in Materials Science (Grant No. JP-MXP0618217637) at ZAIKEN, Waseda University.

---

[1] S. Åsbrink and A. Magnéli, Acta Cryst. **12**, 575 (1959).
[2] L. N. Mulay and W. J. Danley, J. Appl. Phys. **41**, 877 (1970).
[3] S.-H. Hong and S. Åsbrink, Acta Cryst. B **38**, 2570 (1982).
[4] M. Onoda, J. Solid State Chem. **136**, 67 (1998).
[5] S. Ohkoshi, Y. Tsunobuchi, T. Matsuda, K. Hashimoto, A. Namai, F. Hakoe, and H. Tokoro, Nat. Chem. **2**, 539 (2010).
[6] K. Tanaka, T. Nasu, Y. Miyamoto, N. Ozaki, S. Tanaka, T. Nagata, F. Hakoe, M. Yoshikiyo, K. Nakagawa, Y. Umata, K. Imoto, H. Tokoro, A. Namai, and S. Ohkoshi, Cryst. Growth Des. **15**, 653 (2015).
[7] K. Yoshimatsu, O. Sakata, and A. Ohtomo, Sci. Rep. **7**, 12544 (2017).
[8] M. Marezio. D. B. Mcwhan, P. D. Dernier, and J. P. Remeika, J. Solid State Chem. **6**, 213 (1973).
[9] S. Lakkis, C. Schlenker, B. K. Chakraverty, and R. Buder, Phys. Rev. B **14**, 1429 (1976).
[10] M. Taguchi, A. Chainani, M. Matsunami, R. Eguchi, Y. Takata, M. Yabashi, K. Tamasaku, Y. Nishino, T. Ishikawa, S. Tsuda, S. Watanabe, C.-T. Chen, Y. Senba, H. Ohashi, K. Fujiwara, Y. Nakamura, H. Takagi, and S. Shin, Phys. Rev. Lett. **104**, 106401 (2010).

[11] T. Tohyama, R. Ogura, K. Yoshinaga, S. Naito, N. Miyagawa, and E. Kaneshita, J. Phys. Chem. Solids **127**, 252 (2019).
[12] I. E. Grey and J. Ward, J. Solid State Chem. **7**, 300 (1973).
[13] I. E. Grey, C. Li, and I. C. Madsen, J. Solid State Chem. **113**, 62 (1994).
[14] T. Okuda, K. Nakanishi, S. Miyasaka, and Y. Tokura, Phys. Rev. B **63**, 113104 (2001).
[15] S. Ohta, T. Nomura, H. Ohta, and K. Koumoto, J. Appl. Phys. **97**, 034106 (2005).
[16] Y. Yamashita, T. Okuda, S. Mori, Y. Horibe, R. Murata, and T. Katsufuji, Phys. Rev. Mater. **2**, 074409 (2018).
[17] See Supplemental Material at https://link.aps.org/supplemental/10.1103/PhysRevMaterials.4.074401 for the crystal structural parameters, the interatomic bond lengths, the x-ray Laue photographs, and the anisotropy in magnetization and resistivity.
[18] N. Mori, H. Takahashi, and N. Takeshita, High Press. Res. **24**, 225 (2004).
[19] F. Izumi and K. Momma, Solid State Phenom. **130**, 15 (2007).
[20] K. Momma and F. Izumi, J. Appl. Cryst. **44**, 1272 (2011).
[21] C. Schlenker, R. Buder, M. Schlenker, J. F. Houlihan, and L. N. Mulay, Phys. Status Solidi B **54**, 247 (1972).
[22] W. H. Zachariasen, J. Less-Common Met. **62**, 1 (1978).
[23] G. Grüner, Rev. Mod. Phys. **60**, 1129 (1988).
[24] C. Acha, M. Monteverde, M. Núñez-Regueiro, A. Kuhn, and A. M. Alario Franco, Eur. Phys. J. B **34**, 421 (2003).
[25] P. W. Anderson, Mater. Res. Bull. **8**, 153 (1973).
[26] I. Terasaki, Y. Sasago, and K. Uchinokura, Phys. Rev. B **56**, R12685(R) (1997).
[27] M. Cutler and N. F. Mott, Phys. Rev. **181**, 1336 (1969).
[28] B. Fisher, L. Patlagan, G. M. Reiener, and A. Knizhnik, Phys. Rev. B **61**, 470 (2000).
[29] M. Imada, A. Fujimori, and Y. Tokura, Rev. Mod. Phys. **70**, 1039 (1998).